Type of the Paper (Article)

Removal of ethoxylated alkylpehol (NPEG) with TiO_2/ Au catalysts: Kinetic and Initial transformation path

Claudia Aguilar[1,*] Mayra Garcia[1], Carlos Montalvo[1], Edgar Moctezuma,[2] Francisco Anguebes[1], Mohamed Abatal[3], Sandra Figueroa[3]

[1]Universidad Autónoma del Carmen, Facultad de Química Calle 56 No. 4 Av. Concordia, C.P 24180. Ciudad del Carmen, Campeche México; caguilar@pampano.unacar.mx (C.A), maje180894@gmail.com (M.G), cmontalvo@pampano.unacar.mx (C.M), fanguebes@pampano.unacar.mx (F.A).

[2]Universidad Autónoma de San Luis Potosí, Facultad de Ciencias Químicas Av. Dr. Manuel Nava No.6, Zona Universitaria, C.P. 78210. San Luis Potosí, S.L.P., México; edgar@uaslp.mx (E.M)

3 Universidad Autónoma del Carmen, Facultad de Ingeniería Avenida Central S/N, Mundo Maya, C.P 24115. Ciudad del Carmen, Campeche, México; mabatal@pampano.unacar.mx, (M.A), sfigueroa@pampano.unacar.mx (S.F)

*Correspondence: Claudia Aguilar (C.A) alejandra175@hotmail.com; caguilar@pampano.unacar.mx

Abstract: Gold nanoparticles, were deposited in titanium oxide (TiO_2) Degussa-P25 with the Photodeposition method in the presence of UV light at different concentrations. It was determined by diffuse reflectance (DF), Scanning electron microscopy (SEM), that the Photodeposition method is effective for the inclusion of gold particles on the surface. The catalyst band gap showed a reduction to 2.9 e.V, as well as it was observed that the gold-doped catalyst shows absorption in the visible light range around 500 to 600 nm. The percentage of deposited gold nanoparticles was determined by energy dispersive spectroscopy (EDS). The experimental data were analyzed using different analytical techniques (UV-Vis spectrophotometry, TOC total organic carbon), with these results a carbon-based mass balance and reaction kinetics were generated using the Langmuir-Hinshelwood (LH-HW) heterogeneous catalysis model. For the estimation of the kinetic constants, the non-linear regression of the Levengerd Marquad algorithm was used, with these results, kinetic models of the degradation of the molecule and the generation and consumption of Organic Intermediate Products (OIP) were generated.

Keywords: photocatalytic degradation, ethoxylated alkylphenols, gold titanium catalyst

1. Introduction

Today, many compounds are classified as emerging pollutants, including drugs, personal hygiene products, among others [1] a special class of these pollutants are alkylphenol ethoxylates (APEs); its use is related to the plastics industry and as a surfactant in numerous commercial products. Recent studies have shown the presence of alkilphenols and their derivatives in sediments and waters; although the authors consider that the risk factors for the organisms are still low; the potential danger from the increase in these compounds may be of utmost importance in the following years [2], Likewise [3] also report concentrations of these components in different substrates, their studies find a direct relationship between months with low rainfall [4]. Biodegradation of alkylphenol ethoxylates (APEs) during wastewater treatment or subsequent discharge into the environment can

result in small ethoxy chains giving way to hydrophobic metabolites, their biodegradation results in the production of nonylphenol-mono and di-ethoxylated, nonylphenoxy ethoxyacetic acid and nonylphenol, which is more recalcitrant and more toxic than the other nonylphenols (NPEOs) precursors [5].

The reviews by Priac [6] describe different processes for the elimination of emerging contaminants, mainly Alkylphenols and their polyethoxylated derivatives.The technologies proposed for alkylphenol treatment include membrane treatment using biological (membrane bioreactors) or physical processes (membrane filtration such as nanofiltration), biotechnological-based methods (biofilms, immobilized enzymes, etc.), adsorption-oriented processes using conventional (activated carbons) or nonconventional adsorbents (clays, cyclodextrin, etc.), and advanced oxidation processes (photocatalysis, photolysis, and sonochemistry). Photocatalytic oxidation is an interesting tool for alkylphenol treatment due to its potential to reach complete mineralization.

Although the toxicity of (APEs) is relatively low, its study has increased in recent years because its biodegradation is slow and generates highly stable, toxic and bio-recalcitrant secondary products, especially those that have one or two ethoxylated groups, such as nonylphenols and octylphenols as the ability of these compounds to mimic the natural functions of hormones and behave as endocrine disruptors have been demonstrated [5]. Its presence in treatment plants that use microorganisms for the reduction of organic matter causes serious problems due to its ability to produce foams, decrease the capacity of oxygen transfer and disturb primary sedimentation processes, thus making its biodegradation inefficient and incomplete.

Conventional treatments are inadequate or deficient for the degradation of these relatively new pollutants, so several technologies have been proposed for removal, such as membrane-based processes, biotechnological methods, oriented adsorption, and advanced oxidation processes [7] Photocatalytic processes have proven to be highly efficient in the removal of emerging pollutants, including the development of new and innovative reactors [8,9].

Even though photocatalysis has proven to be an efficient process for the removal of organic molecules, "*charge recombination*" decreases the process efficiency [10] in this regard, catalyst doping is an efficient means to achieve deposition of metallic species on the catalyst surface in order to change its electrical properties and increase its efficiency for photocatalytic processes. For these purposes TiO_2 is support for metal ions, its structure consists of small nano-metric particles, which represent a large surface area in which metallic silver can be deposited, which in addition to avoiding recombination (due to the sequestration of electrons from the valence band), makes the photo-generated holes available for the photocatalytic reaction [11]. The effect of gold on different semiconductors and nanocomposites shows an increase in the transformation of the specific surface that improves the photocatalytic activity and improves the separation of the electron-hole pair [12,13].

Particularly, gold nanoparticles have been used as photocatalysts in the degradation of dyes [14-15], and the degradation of phenol and phenol compounds [2,12,13,16] In this sense; [17] shows the presence of gold on TiO_2 facilitates both the electron transfer to O_2 and the mineralization of formic acid, which mainly proceeds through direct interaction with photoproduced valence band holes. The so-formed highly reductant intermediate species may contribute in maintaining gold in metallic form. The controversial results obtained in the photocatalytic degradation of the dye were rationalised by taking into account that with this substrate, which mainly

undergoes oxidation through a hydroxyl radical mediated mechanism, the photogenerated holes may partly oxidise gold nanoparticles, which consequently act as recombination centres of photoproduced charge carriers.

For these reasons, researchers have recently focused on supporting gold nanoparticles on titanium dioxide, which is a promising system for photocatalytic reactions and wastewater treatment. Due to the importance of these compounds and their adverse effects on human health, which is mainly the ability to imitate processes of the endocrine system of different organisms and their degradation mechanisms; advanced treatments are a viable alternative for the removal of NPEG, the study of its reaction kinetics represents an advance in the understanding of the phenomena that lead to the elimination of this component by means of chemical transformation.

2. Results and Discussion

2.1. Preparation and characterization of the catalysts

The calcination process is essential to define the characteristics of the semiconductor. Temperature of 550°C, has been reported in other studies as the optimum in a doping process [18]. The effect of calcination on the photocatalytic activity of Au-TiO_2 has been investigated in some reports. For oxidation of dyes, the photocatalysts calcined at temperatures about 550–625°C, exhibited slightly higher activities that of calcined at higher temperatures. It is probably due to a larger amount of anatase than photocatalysts calcined at higher temperatures [19].

Other studies have shown that the degradation rate increases, with increasing the calcination temperature at the beginning. It has a downtrend after optimum temperature of 300°C. They described that the crystalline size of Au-NPs has direct relationship to the calcination temperature. It is logical to consideran appropriate diameter which is necessary to access high photocatalytic activity [20].

2.1.2 SEM and EDS

The superficial morphological analysis for secondary electrons and chemical analysis by energy dispersive spectroscopy (EDS) was carried out in a Sweeping Dual Beam (FIB/SEM) Electron Microscope FEI-Helios Nanolab 600 .

The scanning electron microscopy in order to observe the superficial morphology and elemental analysis of the catalyst was used, to differentiate the chemical composition of the catalyst was used EDS, fractions of titanium, oxygen and silver are shown in the results (Figure 1 and Figure 2). During the calcination the dispersed ions of Au^{+} gradually migrate to the surface of the TiO_2 to improve the shape of the Crystal resulting in gold deposited on the surface. The transfer of the electron in the conduction band of the titanium to the metallic gold particles is possible, because the Fermi energy level of the titanium is greater than the gold, giving place to the formation of the Schottky barrier in the contact region of Au-TiO_2 which improved the photocatalytic activity.

Small particles of Au may induce greater changes in the Fermi level compared to particles with larger diameters [16, 21] other than agrees that the method Photo-deposition is usually effective by generating smaller particles than those generated by other methods and the catalysts prepared by this method. Were more efficient compared to other methods of inclusion of gold nanoparticles in the catalyst; this behavior may be because titanium behaves as electron deposit when subjected to

Preprints (www.preprints.org) | NOT PEER-REVIEWED | Posted: 14 August 2020 doi:10.20944/preprints202008.0323.v1

UV radiation and modifies its Fermi energy level, [22] in their studies they show that titanium oxide shows a blue coloration when the electrons are stored in the particles, when it is in contact with gold particles, there is a partial disappearance of blue color as stored electrons are transferred from the titanium oxide to gold nanoparticles.

These changes modify the distribution of charges between semiconductor and nanoparticles; as a result the Fermi energy level changes to negative potentials. Also, in their studies they determine that a change in the energy level observed for TiO_2 - Au indicates improved charge separation and demonstrates its usefulness in improving efficiency in photocatalytic reactions.

In Figure 1 shows the micrographs of the synthesized photocatalysts, which mainly reveal spherical, homogeneously sized TiO_2 crystals. In addition, bright spots corresponding to Au particles with nanometric dimensions are observed are spherically shaped, and are distributed homogeneously on the TiO_2 support

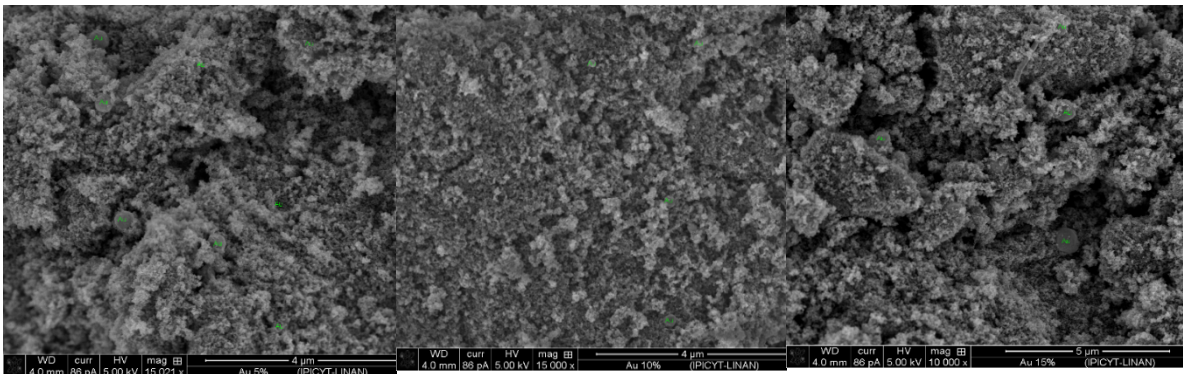

(a) (b) (c)

Figure 1. Scanning electron microscopy images of titanium catalysts doped with gold nanoparticles. (**a**) Microscopy image showing the surface of the catalyst with a concentration of 5% (theoretical) of deposited gold; (**b**); Microscopy image showing the surface of the catalyst with a concentration of 10% (theoretical) of deposited gold. (c) Microscopy image showing the surface of the catalyst with a concentration of 15% (theoretical) of deposited gold.

Preprints (www.preprints.org) | NOT PEER-REVIEWED | Posted: 14 August 2020 doi:10.20944/preprints202008.0323.v1

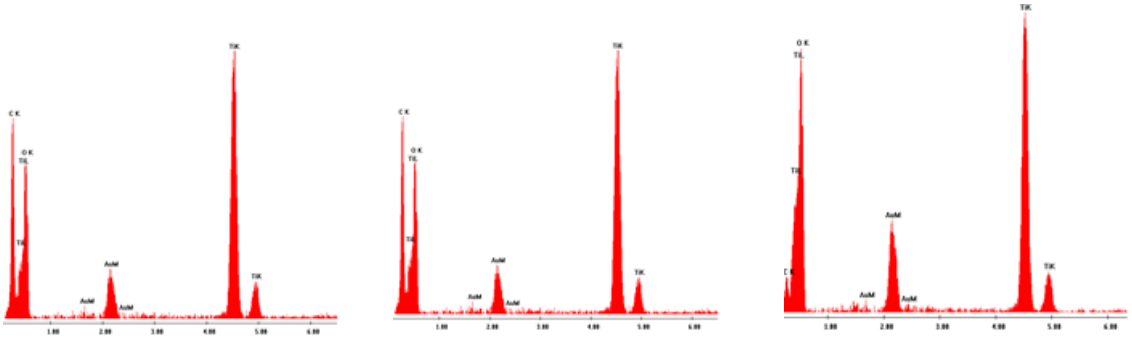

(a) (b) (c)

Figure 2. Elemental composition of the catalysts doped with gold nanoparticles percentages by weight deposited on TiO_2 P-25 catalyst and determined by EDS (**a**); (Wt %) O_2=43.52, Au=2.62, Ti=53.86; (**b**) (Wt %) O_2=44.77, Au=5.4, Ti=49.83; **(c)** (Wt %) O_2=43.85, Au=12.75 Ti=43.40

2.1.3 Surface area

The Figure 3, shows the typical nitrogen adsorption-desorption isotherms of the samples analyzed, which are based on the BET (Brunauer, Emmett y Teller) isotherm, in addition to determining the surface area, the total pore volume and average pore diameter are also determined; superficial area (M^2/g)= 47.57; Vm (Cm^3/g)= 10.931; Total pore volume (Cm^3/g)= 0.3648; Average pore diameter (nm)=30.668.

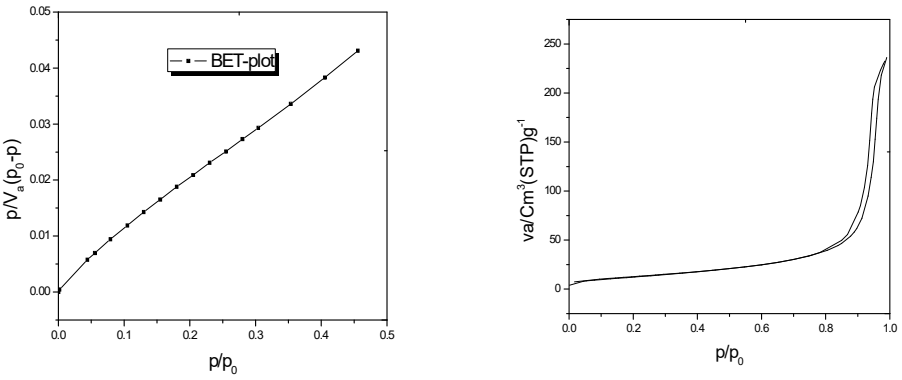

(a) (b)

Figure 3. Adsorption isotherms desorption of the catalyst by Nitrogen Physisorption (**a**) curve of the BET isotherm; (**b**) Desorption/adsorption curve for surface area determination

2.1.4 Diffuse reflectance

The catalysts were analyzed by UV spectroscopy using a Shimadzu UV-2450 equipment, provided with ISR-2200 Integrating Sphere Attachment. Measurements were taken in the range of wavelength between 200 and 600 nm, the spectra determines the dispersion state of the present superficial active species in the catalysts.

Preprints (www.preprints.org) | NOT PEER-REVIEWED | Posted: 14 August 2020 doi:10.20944/preprints202008.0323.v1

In Figure 4 (a) is shown the modifications of the optical properties of titanium by the presence of gold nanoparticles in the surface, it is shown a significant improvement of the absorption due to the surface plasmon resonance between 500 and 600 nm, this behavior is due to the interaction of the metal particles with the incident light; as well as the band gap moves to the visible region.

The role of the efficiency of the photocatalysts by the inclusion of metallic particles like gold can be set for the levels of the Fermi energy, which is displaced to close values to the low part of the conduction band, the accumulation of electrons influences in the absorption of plasmons band. Which can improve the photocatalytic activity of the material in the visible region.

Plasmons play an important role in the optical properties of metals; a plasmon is a quantum phenomenon that results from the interaction of electromagnetic radiation with the interface between a metal and a semiconductor, in most metals the plasma frequency falls into the ultraviolet making them bright in the visible range, in the case of gold, the plasma frequency falls on the deep ultraviolet but the geometric factors reduce the frequency to the visible as in the case of nanoparticles. Therefore, it is possible to observe them in this range.

For the calculation of the band gap, (Table 1) is possible to use the diffuse reflectance spectra to determine the Band gap of powder semiconductors, wavelength data are transformed to frequency through the equation $v = \frac{c}{\lambda_g}$ and it was represented $(Abs * hv)^{\frac{1}{2}}$ in function of hv, Figure 4 (b) through extrapolation of a straight line toward the x-axis from the generated chart, the value of the band gap is determined $E_g = \frac{hc}{\lambda_g} = \frac{h(v\lambda_g)}{\lambda_g} = hv$ Where: λ_g = Wavelength (nm), h = Planck constant, c = Speed of light in vacuum

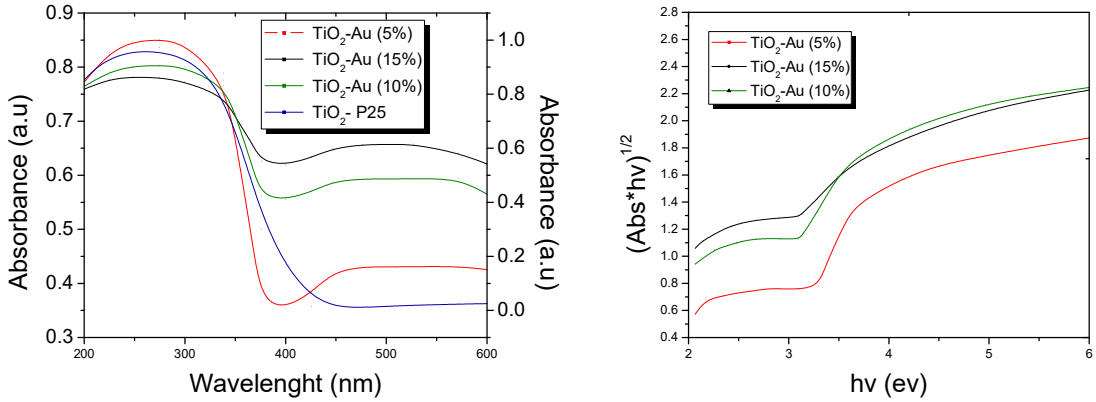

(a) (b)

Figure 4. (a) Kubelka Munk plots of the Au-TiO_2 catalysts**; (b)** Normalization of diffuse reflectance data for band gap calculation

Preprints (www.preprints.org) | NOT PEER-REVIEWED | Posted: 14 August 2020 doi:10.20944/preprints202008.0323.v1

Table 1. Values of the band gap (Eg)

Catalyst	Eg (ev)
Au-TiO_2 at 5%	2.9
Au-TiO_2 at 10%	2.9
Au-TiO_2 at 15%	2.9
TiO_2 P-25	3.1

The mass of the dopant does not influence the estimation of the value of its band gap which was estimated at 2.9 achieving the reduction in comparison with the TiO_2 P-25. In this work it was shown that the theoretical amount deposited in the solid does not correspond to the actual amount deposited and that the temperature at which the solid is calcined is indispensable to ensure that the crystalline structure is not significantly affected.

2.2 Kinetics of Photocatalytic Degradation

The effect of the initial concentration of NPEG on the reaction rate of phodegradation was also investigated, seeing that the concentration of the reactant is a very important variable in the processes of photocatalytic oxidation for that, experiments of different initial concentrations of between 20 and 160 Mg/L were carried out, setting the weight of the catalyst (0.2 g of TiO_2 / 100 mL of solution), the catalyst mass was fixed at 2 g/L, and showed better conversion. A high conversion and high initial rates are achieved in the pollutant elimination when the mass-volume ratio of the photocatalyst in the suspension is the lowest [12]

The volume of the solution (250 mL) and the flow of oxygen (100 mL/min). In all the cases, samples of the reaction mixture were taken for analysis with UV and TOC. The results for these experiments shows in Figures 5 (a), which show the NPEG concentration and total amount of organic carbon as a function of reaction time.

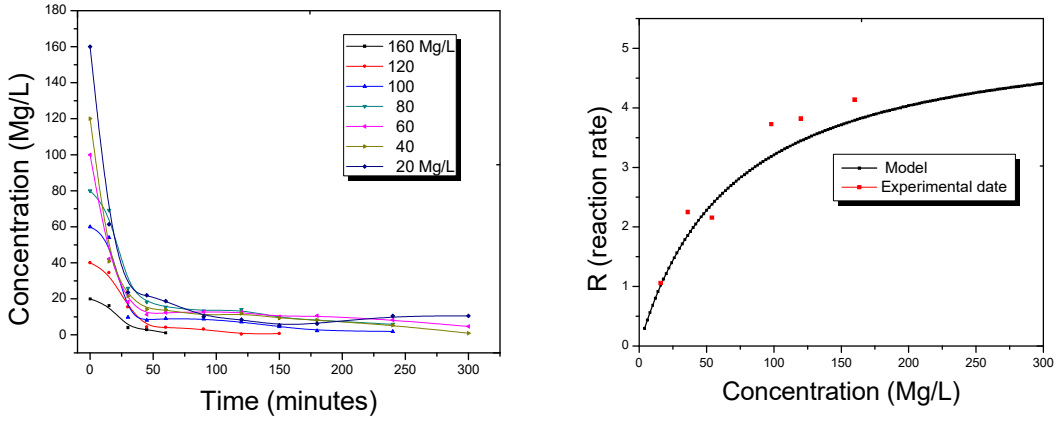

(a) (b)

Figure 5. (a) NPEG concentration (Mg/L) as a function of time, Degradation profile at different reaction times, the curves show the chemical degradation of the molecule from the initial time (time

Preprints (www.preprints.org) | NOT PEER-REVIEWED | Posted: 14 August 2020 doi:10.20944/preprints202008.0323.v1

zero) to the final reaction time of 300 minutes (catalyst concentration = 2 g/L, total volume= 250 ML, amount of oxygen = 100 cm^3/min); (b) Estimation of the LH model applied in the NPEG degradation reaction minutes (catalyst concentration = 2 g/L, $total\ volume = 250\ ML, amount\ of\ oxygen = 100\ cm3/min$)

The initial concentration dependence of the photocatalytic degradation rate of NPEG based on the fact that the degradation reaction occurs on TiO_2 molecules as well as in solution. On the surface of TiO_2 molecules, the reaction occurs between the HO· radicals generated at the active OH sites and NPEG molecule from the solution. When the initial concentration is high, the number of these available active sites is decreased by NPEG molecules because of their competitive absorption of TiO_2 molecules. In this case, the transfer rate of NPEG molecules from the solution does not affect the degradation rate. Several experimental results indicated that the destruction rates of photocatalytic oxidation of various organic contaminants over illuminated TiO_2 fitted the LH-HW model [11, 23].

$$-r_{NPEG} = -\frac{dC_{NPEG}}{dt} = \frac{K_1 C_{NPEG}}{1 + K_2 C_{NPEG} + \sum K_i C_{OIP}} \quad (1)$$

If one analyzes the experimental data in short reaction times, it is possible to overlook the absorption term for the intermediate products. The kinetics constant K_1 and K_2 were calculated by non linear regression; the values for the constant K_1 and K_2 are 0.07848062 (min^{-1}) and 0.1444828 (Mg/L) respectively.

In order to validate the Langmuir- Hinshelwood model. The experimental reaction rates and the reaction rates calculated with equation (1) modified (without the OIP factor), were plotted on Figure 5 (b). Experimental data were also evaluated taking into account a serial kinetics

The degradation reaction behavior of the NPEG molecule presented its main variations in initial reaction times in the first fifty minutes; for this reason, it is considered that Langmuir's model is usually not sufficient to evaluate its kinetics; so it is considered that the model to follow could be that of a first-order reaction; that by its characteristics could be considered a serial reaction, so it was evaluated taking into account overall kinetics for which was initiated with the following approach:

$$A \rightarrow OIP \rightarrow C \quad (2)$$

Where A: Nonylphenol polyethylene glycol (NPEG), organic intermediate products (OIP) and C: CO_2. For the evaluation of NPEG decomposition, a kinetic of the first order is taken to be expressed in equation 3

$$-\frac{dC_A}{dt} = k_1 C_A \quad (3) \qquad C_A = C_{A_0} e^{-k_1 t} \quad (4)$$

Under the same linear method, the formation of OIP can be represented from the following equation:

Preprints (www.preprints.org) | NOT PEER-REVIEWED | Posted: 14 August 2020 doi:10.20944/preprints202008.0323.v1

243 $$\frac{dC_{OIP}}{dt} + k_2 C_{OIP} = k_1 C_{A_0} e^{-k_1 t} \quad (5), \qquad C_{POI} = \frac{k_1 C_{A_0}}{k_2 - k_1} e^{-k_1 t} \quad (6)$$

244 The formation of the final product CO_2 is also evaluated, with equation 7.

245 $$\frac{dC_C}{dt} = k_2 C_{OIP} \quad (7) \qquad t C_C = \frac{k_2 C_{A_0}}{k_1 - k_2} e^{-k_1 t} \quad (8)$$

246 The value of the constants K_1 and K_2 was calculated based on non-linear regression using the
247 Levengerd Marquad algorithm from the statistical package "*Statistical 7.1*"

248 The concentration of the organic intermediate products was calculated based on a mass balance,
249 using the results obtained from the evaluation of the NPEG concentration at different reaction times
250 and TOC values, (Figure 6). The data were obtained by UV spectroscopy; and the mineralization
251 behavior followed by TOC. These two parameters were useful to make the estimation and to obtain
252 the average OIP curve using the equation:

253 $TOC = C_{CARBON}\,NPEG + C_{CARBON}\,OIP$ (9);

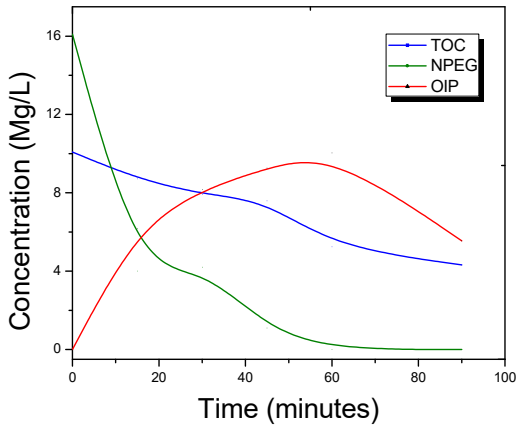

254

255 **Figure 6**. Concentration profile at different reaction times, showing the reaction behavior based on
256 mass balances and total organic carbon profiles (TOC = total organic carbon, NPEG = concentration
257 measured by UV spectroscopy, OIP = organic intermediate products).

258 The results of the application of equation (4) for NPEG degradation are shown in Figure 7, as well as
259 the results for predicting and consuming the formation and consumption of the OIP (equation6) are
260 shown in Figure 8.

Preprints (www.preprints.org) | NOT PEER-REVIEWED | Posted: 14 August 2020 doi:10.20944/preprints202008.0323.v1

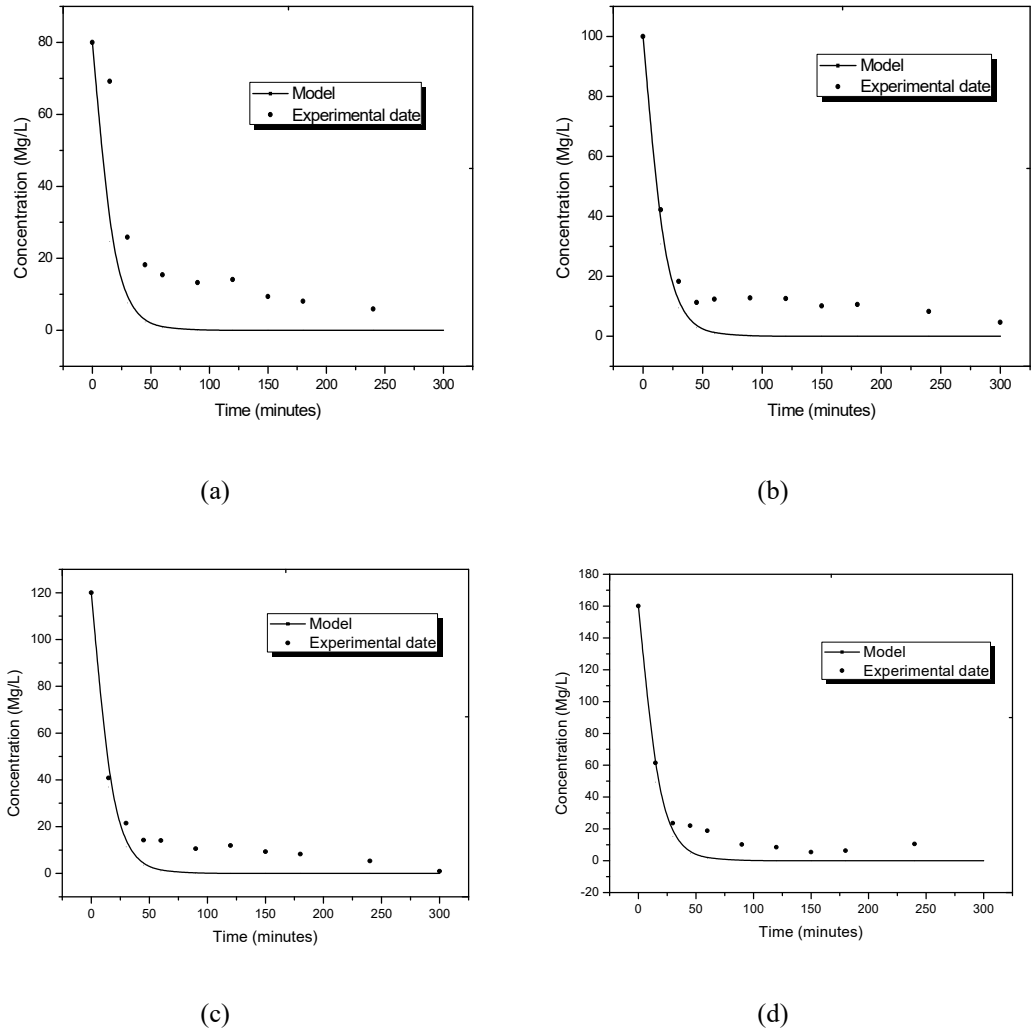

Figure 7. NPEG degradation profile at different concentrations (a) 80 Mg / L, (b) 100 Mg / L, (c) 120 Mg / L, (d) 160 Mg / L, the curve generated with the application of the first-order model is shown and the experimental data obtained by UV-Vis spectroscopy.

Figure 8. Profile of the generation and consumption of organic intermediate products (OIP) shows the curve generated by the model and experimental data obtained by a carbon-based mass balance at different initial concentrations (a) 80 Mg / L, (b) 100 Mg / L (c) 120 Mg / L, (d) 160 Mg / L

However the equation for predicting CO_2 formation it cannot be modeled under first-order kinetics with a serial reaction; this behavior is because there are losses to the atmosphere that cannot be quantified with the analytical tools available; however, the first-order model adequately predicts the degradation of NPEG, as well as the formation and consumption of OIPs; with the results

Preprints (www.preprints.org) | NOT PEER-REVIEWED | Posted: 14 August 2020 doi:10.20944/preprints202008.0323.v1

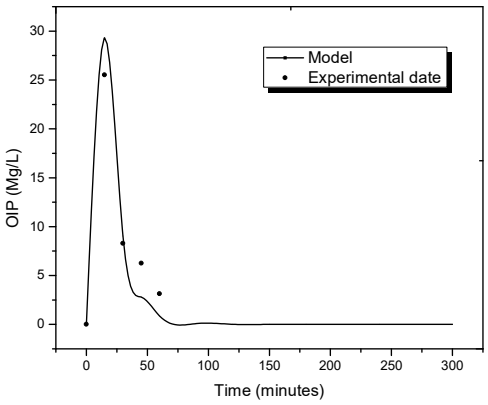

(a)

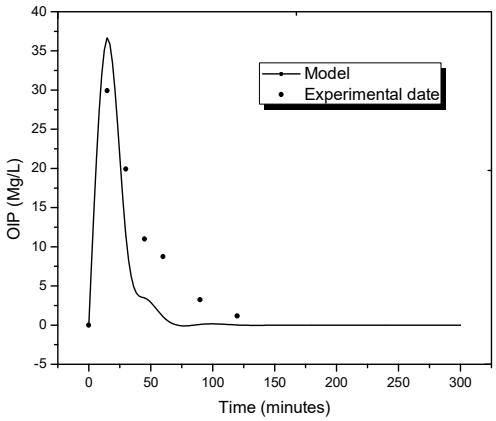

(b)

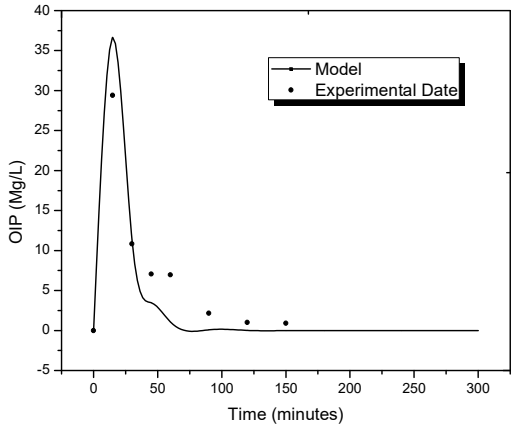

(c)

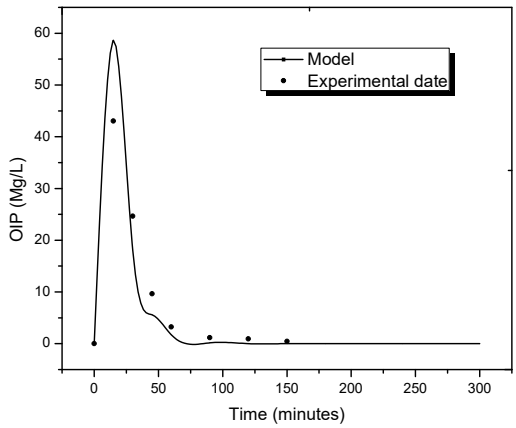

(d)

obtained, it is concluded that the degradation of NPEG as the formation and consumption of the OIP follow first-order kinetics which can be seen in the concentration decrease profile that is observed in all the reactions, which have a considerable decrease during the first 50 minutes and then the reaction becomes pseudo-stationary.

In order to establish the OIP that are formed and consumed during the reaction, FTIR tests were carried out; reaction samples were treated with ethyl acetate and using Micro Extraction in Solid Phase with Licrohout cartridges and analyzed in an FT-IR.

2.2.1 Intermediate products of the reaction

The equipment used was an FTIR spectrophotometer from the Agilent Technologies-Cary 600 brand in conjunction with a GladiATR from the Pike Technologies brand. (UNACAR, Ciudad del Carmen, México)

Figure 9 (a) shows the spectra obtained at the initial reaction time and with four hours of reaction. In the spectrum (A) the presence of 4-nonylphenyl-PEG functional groups can be confirmed. Comparisons of these results with those obtained in spectra (Figure 9 b) at different reaction times show the permanence of the disubstituted aromatic group (669 and 942 cm-1) and its isomerization

 doi:10.20944/preprints202008.0323.v1

289 (868 cm-1); likewise, the functional groups belonging to C-O-R (1014 cm-1) and R-OH (1115 cm-1)
290 persist, indicating a fragmentation of the ethoxylate chain.

291 The formation of carboxylic acids at a wavelength between 1136-1250cm-1, 2540-2690 cm^{-1} and
292 3000-3400 cm^{-1} is highlighted, the latter being also representative for the possible exit of the ethoxylate
293 functional group giving way to the generation of phenols or R-OH groups. Table 3 lists, for
294 comparison, the information obtained in the spectra before and after photodegradation at 300 ppm.

295 The evidences suggest the degradation of the aromatic group and which is evidenced in the UV
296 spectra after two hours of reaction corresponding to a type of $\pi - \pi^*$ transition of the double bond of
297 the aromatic ring; different transformations occurring with molecules of alkylphenol ethoxylates
298 (APEs), in water treatment systems in aerobic and anaerobic conditions; both processes show the
299 initial loss of ethoxylate groups and then the generation of secondary compounds [24] which are
300 more lipophilic and toxic than the original compounds and their carboxylated derivatives. The
301 products formed undergone direct photolysis upon exposed to UV [25] The degradation pathway
302 was complex. Besides the generally proposed degradation pathway of ethylene oxide (EO) side
303 chains shortening, the oxidation of the alkyl chain and EO chain led to intermediates having both a
304 carboxylated (as well as carbonylated) ethoxylate and alkyl chain of varying lengths.

305 **Table 3.** Summary of the structures detected by FT-IR in a NPEG reaction sample

Wavelength (cm^{-1})	Functional group
835	Aromatic for disubstituted
1102,1189	R-OH
1250	C-O-R
1350	R-OH
1450-2000	Aromatic ring
2875-2961	C-H
3200-3650	R-OH

306

307

Preprints (www.preprints.org) | NOT PEER-REVIEWED | Posted: 14 August 2020 doi:10.20944/preprints202008.0323.v1

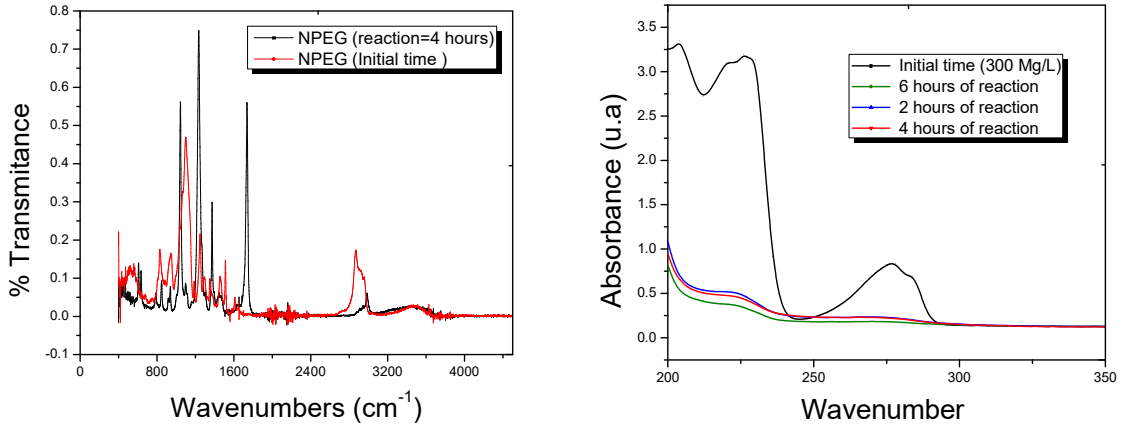

(a) (b)

Figure 9. (a) NPEG FT-IR spectrum at different reaction times; (b) NPEG-UV spectrum at different reaction times

3. Materials and Methods

The catalyst used was titanium oxide (Degussa P-25, Evonik Degussa México S.A de C.V., CDMX, México). 4-Nonylphenyl-polyethylene CAS number: 9016-45-9 was used as a substrate. $HAuCl_4$ PA grade (Sigma Aldrich, Química S.de R.L de C.V,México) was used as a precursor for gold ions. The catalyst separation from the solution was carried out using 0.22 mm cellulose filters (MilliporeCorp, Billerica, MA,US). The surface morphological analysis by secondary electrons and chemical analysis by energy dispersive spectroscopy (EDS), was performed in an FEI-Helios Nanolab 600 Dual Beam Scanning Electron Microscope (FIB / SEM), of the National Lab Research in Nanoscience and Nanotechnology (LINAN, San Luis Potosí, México).To obtain an estimate of the band gap value (E_g) the catalysts were analyzed by UV spectroscopy using a Shimadzu UV-2450 kit, equipped with the ISR-2200 Integrating Sphere Attachment accessory (Autonomous University of San Luis Potosí; UASLP, México).

The surface area was determined with the Belsorp II equipment, at the Civil Engineering Institute of the Autonomous University of Nuevo León Nuevo León; UANL, México. Before analysis, the samples were degassed at a temperature of 300°C for 1 hr. Solid-phase microextraction equipment with Licrohout cartridges was used to extract the organic phase from NPEG reaction samples. SPE has already made remarkable progress compared to LLE in terms of solvent consumption and automation. A step further was achieved by solid-phase microextraction (SPME) and liquid-phase microextraction (LPME), where either no organic solvent is employed (SPME) or only a few microliters (LPME). SPME In this technique , the analytes are first concentrated into a sorbent coated on a fused silica fiber that is exposed directly to the sample (direct sampling) or to its headspace (headspace sampling).

3.1 Photodeposition

The methods of photo deposition are based on certain metal cations with appropriate redox potentials that can be deposited on the support and reduced by photoelectrons created by

semiconductor lighting. One of the additional advantages of this method is that metal during the process is reduced by irradiation with UV.

Precursor salts of $HAuCl_4$ were used to achieve the deposit of gold in the catalyst. For each case in a glass reactor were placed 0.5 g of TiO_2 (Degussa P25) and were added 100 mL of deionized water; to form a homogeneous solution under continuous agitation, initially the solution remained for an hour in dark phase, subsequently the reaction remained for 5 hours with the addition of nitrogen (80 cm^3/min) and the radiation of 4 UV lamps of 365 nm at the end of the reaction period. The water is removed by filtration to vacuum followed by a process of drying at 100° C and calcination at 550°C.

4. Conclusions

The photodeposit method is suitable for embedding gold particles on the surface of the semiconductor; the method is also suitable for reducing metal on the surface in its oxidation state as other studies have indicated; the characteristics of the doped material indicate that the actual percentage of deposited metals is close to the theoretical amount; likewise, the reduction of its band gap makes it suitable for reactions in the presence of visible light; however, the mass of the dopant has no effect on the decrease in bandwidth since this value is the same even when the amount of mass of the gold particle precursor solutions is varied; the surface area if it presents a reduction in comparison with Degussa P-25 the degradation of the NPEG produces an accelerated behavior in the first minutes of the reaction whereby it is considered to evaluate it through the kinetics of a simple first-order reaction. The degradation pathway may begin with the fragmentation of the ethoxylated chain and the subsequent degradation of the aromatic ring.

Author Contributions: **In this paper,** C.A and C.M designed the experiments; M.G performed the experiments; E.M allowed access to specialized equipment to perform the experiments. The manuscript was written by C.A; C.M; F.A, M.A and S.F.

Acknowledgments: To the Autonomous University of Nuevo León (UANL) and Autonomous University of Carmen (UNACAR).

Conflicts of Interest: the authors declare no conflicts of interest

References

1. Ebele, A.J.; Mohamed, A.; Elwafa, A.;Stuart, H. Pharmaceuticals and personal care products (PPCPs) in the freshwater aquatic Environment. *Emerg. Contam*. 2017, 3: 1-16.
2. Diao, P.; Chen, Q.; Wang, R.; Sun, D.; Cai, Z.; Wu., H; Duan, S. Phenolic endocrine-disrupting compounds in the Pearl River Estuary: Ocurrence, bioaccumulation and Risk assessment. *Sci. Total Environ.* 2019, 584: 1100–1107.
3. Huang, B.; Li, X.; Sun, W.; Ren, D.; Li, X.; Liu, Y.; Li, Q.; Pan, X. Occurrence, removal, and fate of progestogens, androgens, estrogens, and phenols in six sewage treatment plants around Dianchi Lake in China. *Environ.Sci. Pollut. Res. Int.*2014, 21: 12898–12908.
4. Cheng, J.R.; Wang, K.; Yu, J.; Yu, Z.; Zhang, Z. Distribution and fate modeling of 4-nonylphenol, 4-t-octylphenol, and bisphenol A in the Yong River of China. *Chemosphere*.2018, 195:594–605.
5. Ying, G.G.; Willians, B.; Kookana, R. Environmental fate of alkylphenols and alkylphenolethoxylates—A review. *Environ. Int.* 2002, 28, 215–226.

6. Priac, A.; Morin-Crini, N.; Druart, C.; Gavoille, S.; Bradu, C.; Lagarrigue, C.; Giangiacomo , G.; Winterton, P.; Crini, G. .Alkylphenol and alkylphenol polyethoxylates in water and wastewater: A review of options for their elimination. *Arab. J. Chem.* 2017, 10 : S3749–S3773.

7. Chung, J.; Lam, S.M.; Mohamed, A.R.; Lee, K.T. Degrading Endocrine Disrupting Chemicals from Wastewater by TiO_2 Photocatalysis: A Review. *Int. J. Photoenergy*.2012, ID-185159: 1-23.

8. Philippe, K.K.; Timmers, R.; Grieken, R.V.; Marugan, J. Photocatalytic Disinfection and Removal of Emerging Pollutants from Efluents of Biological Wastewater Treatments, Using a Newly Developed Large-Scale Solar Simulator. *Ind. Eng. Chem. Res*. 2016,55: 2952–2958.

9. Montalvo, C.; Aguilar, C.A.; Alcocer, R.; Ramirez, M.A.; Cordova, V. A. Semi-Pilot Photocatalytic Rotating Reactor (RFR) with Supported TiO_2/Ag Catalysts for Water Treatment. *Molecules.* 2018,23 (224): 1-11

10. Syrek, K.; Grudzien, J.; Sennik, A.; Brudzisz, A.; Sulka, D. Anodic titanium oxide layers modified with gold, silver and Cooper Nanoparticles. *J. Nanomater.* 2019,ID9208734: 1-10.

11. Aguilar, C.A.; Montalvo, C.; Zermeño, B.B.; Ceron, R.M.; Ceron, J.G.; Anguebes, F.; Ramirez, M.A. Photocatalytic degradation of acetaminophen, tergitol and nonylphenol with catalysts TiO_2/Ag under UV and Vis light. *Int. J. Environ. Sci. Technol.*2018, 16: 843–852.

12. Romero, E.; Gutierrez, M.; Mugica, V.; González, L.; Torres, M.; Tzompantzi, F.J.; Tzompantzi, C. Synthesis and characterization of gold nanoparticles on titanium dioxide for the catalytic degradation of 2, 4 dichlorophenoxyaxetic acid. *J. Appl. Res. Technol.* 2018, 16: 346-356.

13. Ayati, A.; Ahmadpour, A.; Bamoharram, F.; Tanhaei, B.; Manttari, M.; Sillanpaa, M. Review on catalytic applications of Au/TiO_2 nanoparticles in the removal of water pollutant. *Chemosphere.*2014, 107:163–174.

14. Mondal, S.; Reyes, M.E.; Pal, U. Plasmon induced enhanced photocatalytic activity of gold loaded hydroxyapatite nanoparticles for methylene blue degradation under visible light. *RSC advances* . 2017, 7(14): 8633-8645.

15. Sobhana, L.; Sarakha, M.; Prevot, V.; Fardim, O. Layered doublé hidroxides decotared with Au-Pd nanoparticles to photodegradate Orange II from water. *Appl. Clay. Sci.*2016, 134: 120-127.

16. Oros, S.; Pedraza, J.A.; Guzmán, C.; Quintana, M.; Moctezuma, E.; Del angel, G.; Gómez, R.; Pérez, E. Effect of Gold Particle Size and Deposition Method on the Photodegradation of 4-Chlorophenol by Au/TiO_2.*Top. Catal*. 2011, 54: 519–526

17. Dozzi, M.V.; Prati, L.; Canton, P.; Selli, E. Effects of gold nanoparticles deposition on the photocatalytic activity of titanium dioxide under visible light. *Phys. Chem. Chem. Phys.* 2009, 11(33): 71-80.

18. Behpour, M,; Ghoreishi; S.M,; Razavi, S. Photocatalytic activity of TiO_2/Ag nanoparticle on degradation of water pollutions. *Dig J Nanomater Biostruct*.2010, 5: 467–475.

19. Haugen, A.B; Kumakiri, I; Simon, C. TiO_2, TiO_2/Ag and TiO_2/Au photocatalysts prepared by spray pyrolysis. *J. Eur. Ceram. Soc.2011,* 31(3): 291-298.

20. Tian, B.; Zhang, J.; Tong, T.; Chen, F. Preparation of Au/TiO_2 catalysts from Au(I)–thiosulfate complex and study of their photocatalytic activity for the degradation of methyl orange. *Appl. Catal B. Environ.* 2008, 79(4): 394-401.

21. Kamat, P. Photophysical, Photochemical and Photocatalytic Aspects of Metal Nanoparticles. *J. Phys. Chem B.* 2002, 106: 7729–7744

22. Jacob, M.; Levanon, H.; Kamat, P.V. Charge distribution between UV-irradiated TiO_2 and gold nanoparticles: determination of shift in the Fermi level. *Nanoletters*. 2003, 3: 353–358

23. Aguilar, C.; Abatal, M.; Montalvo, C.; Anguebes, F.; Ramírez, M.A.; Cantú, D. Removal of an Ethoxylated Alkylphenol by Adsorption on Zeolites and Photocatalysis with TiO_2/Ag. *Processes.* 2019, 7(889): 1-15.

 doi:10.20944/preprints202008.0323.v1

421 24. Salomon, K.Y.; Huberson, N.G.; Sylvain, A.K. Nonylphenol and Its Ethoxylates in Water Environment.
422 *Journal of Geography, Environ. Earth. Sci.* 2019, 23(4): 1-14.
423 25. Chen, L.; Zhou, H.Y.; Deng, Q.Y. Photolysis of nonylphenol ethoxylates: The determination of the
424 degradation kinetics and the intermediate products. *Chemosphere*.2007, 68:354–359.

425

426
427